Evaluation of a ^{88}Sr$^+$ Optical Clock with a Direct Measurement of the Blackbody Radiation Shift and Determination of the Clock Frequency

M. Steinel,[1] H. Shao,[1] M. Filzinger,[1] B. Lipphardt,[1] M. Brinkmann,[1] A. Didier,[1] T. E. Mehlstäubler,[1,2] T. Lindvall,[3] E. Peik,[1] and N. Huntemann[1,*]

[1]*Physikalisch-Technische Bundesanstalt, Bundesallee 100, 38116 Braunschweig, Germany*
[2]*Leibniz Universität Hannover, Welfengarten 1, 30167 Hannover, Germany*
[3]*VTT Technical Research Centre of Finland Ltd, National Metrology Institute VTT MIKES,*
P.O. Box 1000, 02044 VTT, Finland

We report on an evaluation of an optical clock that uses the $^2S_{1/2} \rightarrow {}^2D_{5/2}$ transition of a single ^{88}Sr$^+$ ion as the reference. In contrast to previous work, we estimate the effective temperature of the blackbody radiation that shifts the reference transition directly during operation from the corresponding frequency shift and the well-characterized sensitivity to thermal radiation. We measure the clock output frequency against an independent ^{171}Yb$^+$ ion clock, based on the $^2S_{1/2}(F=0) \rightarrow {}^2F_{7/2}(F=3)$ electric octupole (E3) transition, and determine the frequency ratio with a total fractional uncertainty of 2.3×10^{-17}. Relying on a previous measurement of the ^{171}Yb$^+$ (E3) clock frequency, we find the absolute frequency of the ^{88}Sr$^+$ clock transition to be 444 779 044 095 485.277(59) Hz. Our result reduces the uncertainty by a factor of 3 compared with the previously most accurate measurement and may help to resolve so far inconsistent determinations of this value. We also show that for three simultaneously interrogated ^{88}Sr$^+$ ions, the increased number causes the expected improvement of the short-term frequency instability of the optical clock without degrading its systematic uncertainty.

Optical clocks have demonstrated record fractional uncertainties on the order of and below 10^{-18} [1,2]. In addition to their development as future primary standards of time and frequency, comparisons between optical clocks have been used to provide stringent tests of fundamental physical principles such as the Einstein equivalence principle [2,3] and were employed in searches for ultralight scalar dark matter [4,5]. Optical clocks based on neutral atoms in optical lattices and on ions confined in radio-frequency traps both show significant contributions to their total uncertainty originating from the uncertainty of the Stark shift induced by thermal radiation. For neutral atoms, the effective temperature of the perturbing field has been determined with high accuracy using resistive temperature sensors at the position of the atoms [6] or using temperature controlled environments with high emissivity [7]. For trapped ions, however, the determination is particularly challenging because of the inhomogeneous distribution of heat and the large uncertainty of the emissivity of the components of an ion trap [8]. Consequently, the

uncertainty of the effective temperature of the perturbing thermal field has been on the order of a few Kelvin for many trapped ion systems [1,8]. This technical limitation has been addressed by proper ion trap engineering using materials with a high thermal conductivity. For such systems, the combination of finite element simulations and measurements using temperature sensors on the trap assembly and infrared cameras enables temperature uncertainties as low as 0.08 K [9,10]. In a complementary approach, the *in situ* temperature measurement reported in this Letter does not require sophisticated techniques but makes direct use of the frequency shift induced by thermal radiation on the $^2S_{1/2} \rightarrow {}^2D_{5/2}$ clock transition at 674 nm of a single trapped ^{88}Sr$^+$ ion. The technique is easily applicable to other ion species like ^{40}Ca$^+$ [11].

For the demonstration of the technique, we employ a linear ion trap made from printed circuit boards of fiber-reinforced hydrocarbon-ceramics (Rogers 4350B). The low heat conductivity of only 0.69 W/(m K) makes an accurate determination of the effective temperature using well-established techniques challenging. The trap geometry is based on the design discussed in [12], that provides several trapping regions with ten individual segments to confine ^{88}Sr$^+$ ions. We apply radio frequency and dc voltages to obtain mean secular trapping frequencies of up to 1320 kHz and 870 kHz in the radial and axial direction, respectively.

The ion is laser cooled to 0.73(12) mK on the 422 nm electric dipole transition, which is 50% larger than the Doppler limitation expected from laser cooling [13], at a detuning of half its natural linewidth (-10 MHz) with respect to the resonance. A repump laser at 1092 nm prevents population trapping in the $^2D_{3/2}$ state and is polarization modulated with a frequency of about 10 MHz to enable fast repumping from all $^2D_{3/2}$ Zeeman sublevels [14].

During clock operation, the clock transition is periodically interrogated with a pulse sequence that is shown in the Supplemental Material [15]. Each sequence starts with 5 ms of laser cooling. State preparation of a single Zeeman sublevel $m_S = -1/2(+1/2)$ of the $^2S_{1/2}$ ground state within 1 ms is implemented by continuously driving the 674 nm $m_S = +1/2(-1/2) \rightarrow m_D = -3/2(+3/2)$ transition respectively, together with 1033 nm repumping [16]. Mechanical shutters block laser light employed for cooling during the subsequent clock interrogation. Their operation causes a dead time of 5 ms at the beginning and the end of the clock interrogation. A successful clock excitation is indicated by absence of fluorescence at the beginning of the subsequent cooling cycle. After 5 ms of fluorescence detection, laser light at 1033 nm enables fast depletion of the excited clock state via the $P_{3/2}$ state back to the ground state. A valid clock interrogation cycle ends with the reappearance of the fluorescence signal within the subsequent cooling period.

To coherently interrogate the ^{88}Sr$^+$ clock transition, we set up a laser system at 674 nm which takes advantage of the low frequency instability of a cryogenic silicon resonator [17] at short averaging times and uses an independent ^{171}Yb$^+$(E3) clock as the long-term reference [2]. An external-cavity diode laser at 674 nm is stabilized with a bandwidth of 500 kHz to a piezo-controlled Fabry-Perot resonator with a finesse of 34 000 using a Pound-Drever-Hall locking scheme [18]. The transmitted light is frequency shifted with an acousto-optic modulator (AOM) by about 80 MHz, and used to injection seed a laser diode. The output power of up to 7 mW is increased to more than 50 mW using a tapered amplifier. A small fraction of the light is sent to a frequency comb generator and compared to the ^{171}Yb$^+$(E3) clock laser light. A discriminator signal is provided using the transfer scheme [19] to steer the AOM and the length of the Fabry-Perot resonator. Apart from a digitally controlled clock offset, the ^{171}Yb$^+$(E3) clock laser is stabilized to the length of the cryogenic resonator via a laser at 1.5 μm making use of the same transfer scheme. An additional AOM provides a digitally controllable frequency offset of the clock laser light at the position of the ^{88}Sr$^+$ ion. For all clock laser beams guided in optical fibers, active path-length stabilization is employed.

Neither the ^{88}Sr$^+$ ground state $S_{1/2}$ nor the excited state $D_{5/2}$ possesses sublevels with a magnetic quantum number

$m = 0$; consequently all of the possible $(S_{1/2}, m = m_S) \rightarrow (D_{5/2}, m = m_D)$ transition frequencies linearly depend on the magnitude of the magnetic field. Since the corresponding frequency shifts of positive and negative Zeeman sublevels of the ground and excited state with the same absolute magnetic quantum numbers $|m_S|$ and $|m_D|$ average to zero, pairs of transitions are interrogated. To avoid low-frequency magnetic field noise, a single-layer mu-metal shield surrounds the vacuum chamber, and low-noise current sources are used to provide a magnetic field of ≈ 4 μT. An angle of 30° between the propagation direction of the horizontally polarized clock laser light and the applied magnetic field leads to a nonzero excitation probability for all transitions with $|\Delta m| \leq 2$.

In addition to the linear Zeeman shift, the excited state sublevels are affected by tensorial frequency shifts, which scale with m_D^2 [20]. These are the electric quadrupole shift, which results from a coupling between electric field gradient and electric quadrupole moment of the excited state, and the tensorial part of the Stark shift resulting from the residual rf trapping field. To suppress tensorial shifts, we average multiple pairs of transitions with positive and negative Zeeman shift and with different m_D^2. The average frequency of transitions to all excited state sublevels is intrinsically free of tensor shifts [21]. In first-order perturbation theory, the same frequency is obtained by averaging only two pairs of transitions using appropriate weights [20]. Since magnetic field noise determines the maximum coherent interrogation time for our setup, we use a numerical optimization to minimize the frequency instability of the clock under the condition of tensor shift cancellation using individually adjusted interrogation pulse durations on each transition pair. We find the lowest frequency instability if the $|S, \pm 1/2\rangle \rightarrow |D, \pm 3/2\rangle$ transition pair is interrogated twice as often as the $|S, \pm 1/2\rangle \rightarrow |D, \pm 5/2\rangle$ transition pair, with pulse durations of 87.5 ms and 35 ms and averaged with weights of 5/6 and 1/6, respectively [15].

The center frequency of each transition involved in the averaging scheme discussed above is tracked individually by an integrating servo system and averaged in postprocessing to obtain the frequency difference between the clock laser and the unperturbed $S_{1/2} \rightarrow D_{5/2}$ transition. Each transition is interrogated with single rectangular clock laser pulses with positive ($+$) and negative ($-$) detunings $\Delta \nu$ from the center frequency, such that the expected excitation probability is 50% of the maximum. The corresponding servo systems shift the center frequencies by $0.15(n_+ - n_-) \times \Delta \nu$ with $n_{+/-}$ being the number of successful excitations after four interrogations [22].

To experimentally investigate the frequency instability of the ^{88}Sr$^+$ clock, we compare it to the ^{171}Yb$^+$(E3) clock [2], which employs the electric octupole (E3) transition at 467 nm. For the latter, a frequency instability of $1 \times 10^{-15}(\tau/s)^{-1/2}$ has recently been reported in

Ref. [23]. Figure 1 shows the fractional Allan deviation σ_y of the frequency ratio $\mathfrak{R} = \nu_{^{88}Sr^+}/\nu_{^{171}Yb^+}$ for a typical measurement run recorded from MJD 59627 to MJD 59634 (17 Feb 2022 to 24 Feb 2022). A Monte Carlo simulation of the servo algorithm assuming only quantum projection noise predicts an instability $\sigma_y = 4.8 \times 10^{-15}(\tau/s)^{-1/2}$, with which the experimental data are in good agreement.

The frequency instability is expected to decrease with $1/\sqrt{N}$ where N is the number of simultaneously interrogated ions. Consequently, the measurement time required to reach a given statistical uncertainty is reduced by N, if the experimental sequence remains otherwise unchanged. This particular advantage of a so-called multi-ion clock [24] can be exploited with ion species that show a small sensitivity to electric field gradients, such as $^{115}In^+$ [24], $^{27}Al^+$ [1], Sn^{2+} [25], Pb^{2+} [26], or other atomic species when multi-ion related shifts are zeroed by dynamic decoupling or state averaging [27,28]. In these cases, fractional frequency uncertainties of 10^{-19} and below can be achieved [29]. To verify the fundamental $1/\sqrt{N}$ scaling for our system, we also operate the clock using the same ion trap with three $^{88}Sr^+$ ions and align the magnetic field at an angle of $54.7(4)°$ to the trap axis to minimize the frequency shift induced by the electric field gradient along the trap axis [28]. The corresponding frequency instability follows $\sigma_y = 3.3 \times 10^{-15}(\tau/s)^{-1/2}$ as shown in Fig. 1. The instability does not decrease by the expected factor $\sqrt{3}$ compared with the single-ion result, because the detection and cooling times were increased to 15 ms each to reliably determine the number of excited ions from the integrated single photon detector counts of all ions. The mean frequency ratio determined
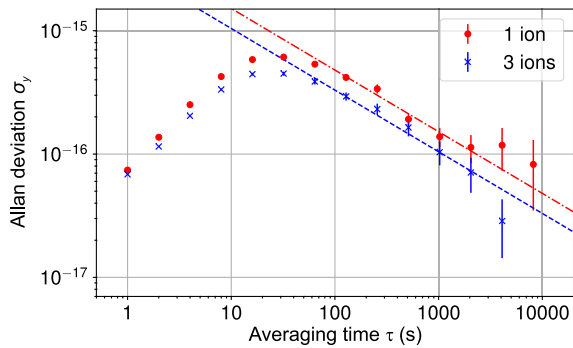

FIG. 1. Fractional instability determined by the Allan deviation σ_y of the frequency ratio $\nu_{^{88}Sr^+}/\nu_{^{171}Yb^+}$ for a single measurement run. The long-term behavior predicted by a Monte Carlo simulation of the servo algorithm assuming quantum projection noise only is indicated by the dashed-dotted line. Also shown is the result of the comparison when the $^{88}Sr^+$ clock is operated with three ions. The corresponding simulation considers the increased detection and cooling time (dashed line).

with three ions agrees with the single-ion result discussed below up to a fractional difference of $2.7(3.3) \times 10^{-17}$.

Shifts considered in the evaluation of the $^{88}Sr^+$ single-ion clock are summarized in Table I. While the dominant shift resulting from thermal radiation is investigated using a novel approach discussed below, the evaluation of all other shift effects follows well-established methods [20]. The second largest shift results from excess micromotion causing Stark and second-order Doppler shifts. The corresponding rf field is determined using the photon correlation technique [30] with a minimum amplitude of 320(70) V/m. It is mainly aligned along the trap axis which prevents a compensation using static electric fields. Because of the negative differential polarizability $\Delta\alpha = -4.7938(71) \times 10^{-40}$ Jm^2/V^2, the second order Doppler and Stark shift cancel out at the so-called magic rf frequency of about 14.4 MHz [31]. For the rf trap drive frequencies of 12.8 MHz and 13.28125 MHz used for the measurements reported here, the relative difference [32] of the absolute values of both shifts is 0.24 and 0.17, respectively. Excess micromotion is minimized and determined before and after each clock run along three noncoplanar orientations. Significant deviations from a constant amplitude over each measurement run have not been observed.

The frequency shifts from thermal ion motion are calculated using the ion temperature inferred from measurements of the relative excitation probability on the carrier and corresponding sideband transitions [33]. For the axial and radial (x, y) directions at secular frequencies of 870 kHz and (1300 kHz, 1330 kHz), we find ion temperatures of 0.5(1) mK and [2.0(3) mK, 2.5(4) mK], respectively. These measurements include the temperature rise during clock interrogation above the initial temperature after Doppler cooling resulting from motional heating of the trapped ion with $dT_{ax}/dt = 0.73(26)$ mK/s and $dT_{rad}/dt = 16.6(2.2)$ mK/s. The large difference in heating rates can result from electric field gradients connected to a not compensable micromotion along the axial direction as discussed in Ref. [34]. While the linear Zeeman shifts average to zero for the clock output signal, they can be employed to determine the quadratic Zeeman shifts on the fly using the sensitivity coefficient given in Ref. [20]. During the clock interrogation, mechanical shutters block all laser beams except the 674 nm clock laser.

We estimate the frequency shift induced by collisions of the trapped ion with background gas molecules from position changes of a two-ion crystal [35]. Our measurements were performed using $^{171}Yb^+$ and $^{174}Yb^+$ in the same ion trap segment and indicate a maximum fractional frequency shift of 5×10^{-19} which we consider as the corresponding uncertainty. Drifts of the magnetic field strength cause a residual shift of the averaged transition frequency, which we estimate using a Monte Carlo simulation of the servo algorithm and find no significant deviation at the uncertainty listed in Table I. AOM chirps

TABLE I. Fractional frequency shifts $\delta\nu/\nu_0$ and corresponding uncertainties $u(\delta\nu)/\nu_0$ considered for the realization of the unperturbed $S_{1/2} \to D_{5/2}$ transition frequency ν_0 of the ^{88}Sr$^+$ single-ion clock for low rf power of the ion trap.

Shift effect	$\delta\nu/\nu_0$ (10^{-18})	$u(\delta\nu)/\nu_0$ (10^{-18})
Blackbody radiation	537.9	7.6
Micromotion	−15.1	6.6
Servo error	0.0	0.7
Collisions	0.0	0.5
Thermal motion	−1.01	0.11
AOM chirp	0.0	0.1
Quadratic Zeeman	0.1409	0.0003
Total	522	10

resulting from the thermal expansion of the crystal during operation have been investigated in Ref. [36] and would cause a maximum shift of 2.4×10^{-18} for our experimental parameters without active suppression. For our setup, however, the clock laser beam features an active optical path length stabilization which is implemented with the nondiffracted part of the light passing the AOM and reflected close to the vacuum chamber [37]. From the integrating servo system with a bandwidth of 10 kHz, we expect a large suppression of the chirp. Thus we do not expect a relevant shift larger than 1×10^{-19}, which we assume as the uncertainty.

The largest deviation between the observed and the unperturbed clock transition frequency is caused by the quadratic Stark shift of thermal radiation, typically referred to as the blackbody radiation (BBR) shift

$$\Delta\nu_{\mathrm{BBR}} = -\frac{1}{2h}\langle E^2(T_{\mathrm{BBR}})\rangle \Delta\alpha_0[1 + \eta(T_{\mathrm{BBR}})], \quad (1)$$

where h is the Planck constant, $\langle E^2(T_{\mathrm{BBR}})\rangle$ is the mean squared electric field of a blackbody at temperature T_{BBR}, $\Delta\alpha_0$ is the static differential polarizability, and $\eta(T_{\mathrm{BBR}})$ corrects for the wavelength dependence of the differential polarizability over the BBR spectrum [38].

The temperature T_{BBR} can be described by the background temperature T_B measured outside the vacuum chamber with accurate temperature sensors with an uncertainty of 0.2 K and the temperature rise ΔT resulting from radio-frequency losses that heat the ion trap assembly during operation. This rise of the effective temperature ΔT is usually determined by finite-element method modeling, complemented with infrared camera observations and sensor measurements [8]. While infrared camera observations require infrared-transparent windows, sensor measurements are only reliable when the trap is made from materials with high thermal conductivity and direct rf-induced heating of the sensors is avoided. These requirements are usually only fulfilled in highly specialized ion

traps [9,10], but here we show that ΔT can also be measured spectroscopically. The spectroscopic determination is particularly important for setups where the heat is predominantly generated inside trap assembly so that it cannot be easily measured outside the vacuum chamber. For moderate temperature increases of the ion trap and negligible heat dissipation via radiation, ΔT is proportional to the power provided by the rf drive P_{rf}. Under these constraints, frequency measurements at different P_{rf} of optical transitions with large, but known BBR shift sensitivity enable extrapolation to $\Delta T = 0$. The frequency shift $\Delta\nu(T_{\mathrm{BBR}})$ at $\Delta T = 0$ can be calculated from T_B independent of the emissivity and geometry of surfaces inside the vacuum chamber, using the realistic assumption that without rf drive the ion trap is inside a closed system in thermal equilibrium.

For ^{88}Sr$^+$, the sensitivity of the clock transition frequency to thermal radiation can be well approximated by $\Delta\nu_{\mathrm{BBR}}(T) = 3.0616(46) \times 10^{-11}$ Hz/K$^4 \times T^4$ at room temperature [31]. Figure 2 shows measurements of the frequency ratio $\mathfrak{R}$ for different settings P/P_0 of the rf drive power of the ^{88}Sr$^+$ ion trap. The systematic shift and corresponding uncertainty is applied to each data point individually to compensate for changes in the uncertainty budget connected to the rf power. The temperature rise of $\Delta T = 0.6(1.0)$ K at P_0 is derived from a least-squares regression of $\mathfrak{R}_T(T_B, P/P_0) = \Delta\nu_{\mathrm{BBR}}(T_B + P/P_0 \times \Delta T)/\nu_{^{171}\mathrm{Yb}^+}$. To improve visibility of the relative change of $\mathfrak{R}_T$ in Fig. 3, data collected for the same T_B and P/P_0 setting are averaged.

Using all data recorded with a single ion, the frequency ratio of the unperturbed ^{88}Sr$^+$ and $^2S_{1/2}(F = 0) \to {}^2F_{7/2}(F = 3)$ ^{171}Yb$^+$(E3) clock transitions is $\mathfrak{R} = 0.692\,671\,163\,215\,966\,059(16)$. A gravitational redshift between the two clocks of $-1.314(31) \times 10^{-17}$ has been taken into account. The total relative uncertainty of
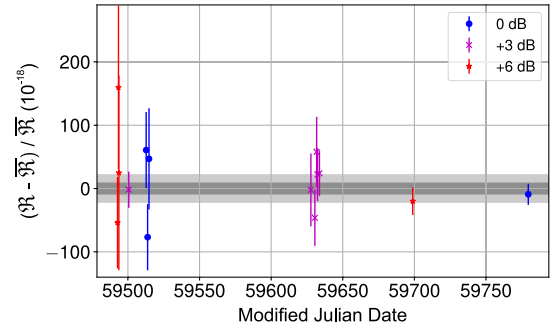

FIG. 2. Measurements of the ratio $\mathfrak{R}$ of the ^{88}Sr$^+$ and ^{171}Yb$^+$(E3) clock frequencies for different settings of the relative ion trap drive powers, distributed over eight months. The error bars indicate the statistical uncertainty. All data are consistent with the weighted mean value $\bar{\mathfrak{R}}$. The gray shaded area shows its statistical uncertainty of 1.0×10^{-17}, and the light gray area corresponds to the total uncertainty (2.3×10^{-17}).
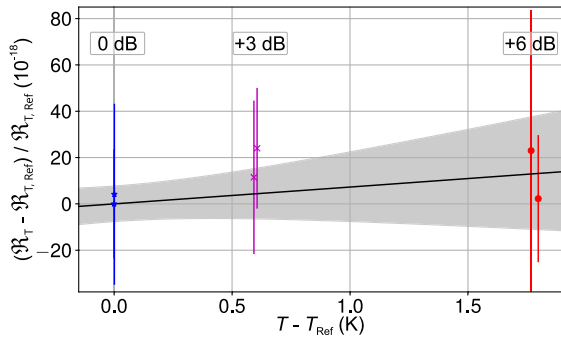
FIG. 3. Relative difference of the frequency ratio $\Re_T$ of the $^{88}\text{Sr}^+$ clock and an independent fully corrected $^{171}\text{Yb}^+$(E3) clock from the measurement with the smallest statistical uncertainty $\Re_{T,\text{Ref}}$. For the $^{88}\text{Sr}^+$ clock all frequency shifts are corrected except for the BBR shift. The ion trap of the $^{88}\text{Sr}^+$ clock is operated with different settings of the relative rf drive power P/P_0, indicated by symbol and color. Changes in T_{BBR} resulting from variations in the ambient temperature T_B for measurements with the same rf power have been corrected for. The BBR shift obtained via least-squares regression is indicated by the black line. The shaded area shows the uncertainty of the BBR shift, where it is assumed that the temperature difference is completely given by the effect of the rf drive. The error bars indicate only statistical uncertainties.

2.3×10^{-17} results from the statistical uncertainty (1.0×10^{-17}) and the systematic uncertainties of the $^{88}\text{Sr}^+$ and $^{171}\text{Yb}^+$(E3) clocks of 2.0×10^{-17} and 2.7×10^{-18} [2], respectively. The total systematic uncertainty is larger than the minimum value reported in Table I due to the larger BBR shift and micromotion uncertainties at the larger rf drive settings.

We calculate the absolute frequency of the $^{88}\text{Sr}^+$ clock transition from $\Re$ and an accurate measurement of the $^{171}\text{Yb}^+$(E3) clock transition frequency previously performed in our laboratory [3] to be $\nu_{^{88}\text{Sr}^+} = 444\,779\,044\,095\,485.277(59)$ Hz. This result is compared
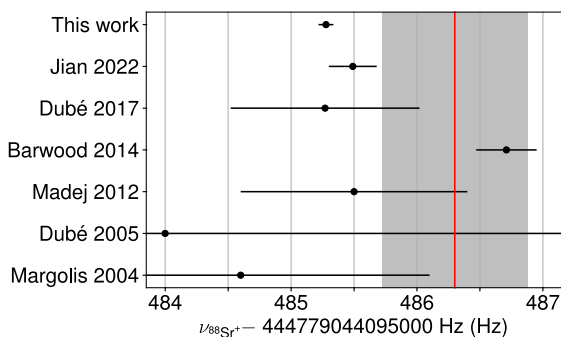

FIG. 4. Results of measurements of the $^{88}\text{Sr}^+$ clock transition frequency obtained in the previous Refs. [21,39–43] and this Letter. The recommended value for $\nu_{^{88}\text{Sr}^+}$ as a secondary representation of the second approved in 2021 [44] is shown by the red line, and the shaded area is its uncertainty.

with previously published values [21,39–43] and the recommended value of the standard frequency [44] in Fig. 4. The previous two most accurate determinations show a discrepancy of 4σ. Our result agrees with all except the determination from Ref. [41], and we improve the total uncertainty compared with the previous most accurate measurement [43] by a factor of 3. This information is particularly relevant for the next adjustment of the recommended value of the standard frequency.

In summary, we have operated an optical clock based on the $^2S_{1/2} \rightarrow {}^2D_{5/2}$ transition of a single trapped $^{88}\text{Sr}^+$ ion to determine its frequency against an independent $^{171}\text{Yb}^+$(E3) clock. The frequency ratio with a fractional uncertainty of 2.3×10^{-17} is among the most precisely measured natural constants to date, and the inferred absolute frequency will support an improved recommended value. This result is particularly important for the practical realization of the System International base unit Hertz with $^{88}\text{Sr}^+$ ion clocks [44]. We have also shown that the clock can be operated with multiple ions to reduce the frequency instability. Our method to determine the effective temperature is directly applicable for various ion species and provides a similar uncertainty like more involved techniques [8]. It is particularly advantageous for clock systems with ancillary transitions that feature a large but known differential polarizability such as $^{27}\text{Al}^+/^{40}\text{Ca}^+$ [11,45], $^{176}\text{Lu}^+$ [46], and $^{115}\text{In}^+/^{172}\text{Yb}^+$ [47].

---

*nils.huntemann@ptb.de

[1] S. M. Brewer, J.-S. Chen, A. M. Hankin, E. R. Clements, C. W. Chou, D. J. Wineland, D. B. Hume, and D. R. Leibrandt, Phys. Rev. Lett. **123**, 033201 (2019).

[2] C. Sanner, N. Huntemann, R. Lange, C. Tamm, E. Peik, M. S. Safronova, and S. G. Porsev, Nature (London) **567**, 204 (2019).

[3] R. Lange, N. Huntemann, J. M. Rahm, C. Sanner, H. Shao, B. Lipphardt, C. Tamm, S. Weyers, and E. Peik, Phys. Rev. Lett. **126**, 011102 (2021).

[4] B. M. Roberts *et al.*, New J. Phys. **22**, 093010 (2020).

[5] Boulder Atomic Clock Optical Network (BACON) Collaboration, Nature (London) **591**, 564 (2021).

[6] B. J. Bloom, T. L. Nicholson, J. R. Williams, S. L. Campbell, M. Bishof, X. Zhang, W. Zhang, S. L. Bromley, and J. Ye, Nature (London) **506**, 71 (2014).

[7] K. Beloy, N. Hinkley, N. B. Phillips, J. A. Sherman, M. Schioppo, J. Lehman, A. Feldman, L. M. Hanssen, C. W. Oates, and A. D. Ludlow, Phys. Rev. Lett. **113,** 260801 (2014).

[8] M. Doležal, P. Balling, P. B. R. Nisbet-Jones, S. A. King, J. M. Jones, H. A. Klein, P. Gill, T. Lindvall, A. E. Wallin, M. Merimaa, C. Tamm, C. Sanner, N. Huntemann, N. Scharnhorst, I. D. Leroux, P. O. Schmidt, T. Burgermeister, T. E. Mehlstäubler, and E. Peik, Metrologia **52,** 842 (2015).

[9] T. Nordmann, A. Didier, M. Doležal, P. Balling, T. Burgermeister, and T. E. Mehlstäubler, Rev. Sci. Instrum. **91,** 111301 (2020).

[10] P. B. R. Nisbet-Jones, S. A. King, J. M. Jones, R. M. Godun, C. F. A. Baynham, K. Bongs, M. Doležal, P. Balling, and P. Gill, Appl. Phys. B **122,** 1 (2016).

[11] Y. Huang, H. Guan, M. Zeng, L. Tang, and K. Gao, Phys. Rev. A **99,** 011401(R) (2019).

[12] K. Pyka, N. Herschbach, J. Keller, and T. E. Mehlstäubler, Appl. Phys. B **114,** 231 (2014).

[13] A. A. Madej and J. E. Bernard, in *Frequency Measurement and Control*, Topics in Applied Physics Vol. 79, edited by A. N. Luiten (Springer, Berlin, Heidelberg, New York, 2001), pp. 153–194, 10.1007/3-540-44991-4_7.

[14] T. Lindvall, M. Merimaa, I. Tittonen, and A. A. Madej, Phys. Rev. A **86,** 033403 (2012).

[15] See Supplemental Material at http://link.aps.org/supplemental/10.1103/PhysRevLett.131.083002 for the derivation of the interrogation sequence optimized for minimal instability and a diagram of the overall pulse sequence used for the experiment.

[16] C. F. Roos, M. Chwalla, K. Kim, M. Riebe, and R. Blatt, Nature (London) **443,** 316 (2006).

[17] D. G. Matei, T. Legero, S. Häfner, C. Grebing, R. Weyrich, W. Zhang, L. Sonderhouse, J. M. Robinson, J. Ye, F. Riehle, and U. Sterr, Phys. Rev. Lett. **118,** 263202 (2017).

[18] R. W. P. Drever, J. L. Hall, F. V. Kowalski, J. Hough, G. M. Ford, A. J. Munley, and H. Ward, Appl. Phys. B **31,** 97 (1983).

[19] H. R. Telle, B. Lipphardt, and J. Stenger, Appl. Phys. B **74,** 1 (2002).

[20] P. Dubé, A. A. Madej, Z. Zhou, and J. E. Bernard, Phys. Rev. A **87,** 023806 (2013).

[21] P. Dubé, A. A. Madej, J. E. Bernard, L. Marmet, J.-S. Boulanger, and S. Cundy, Phys. Rev. Lett. **95,** 033001 (2005).

[22] E. Peik, T. Schneider, and C. Tamm, J. Phys. B **39,** 145 (2006).

[23] S. Dörscher, N. Huntemann, R. Schwarz, R. Lange, E. Benkler, B. Lipphardt, U. Sterr, E. Peik, and C. Lisdat, Metrologia **58,** 015005 (2021).

[24] N. Herschbach, K. Pyka, J. Keller, and T. E. Mehlstäubler, Appl. Phys. B **107,** 891 (2012).

[25] D. R. Leibrandt, S. G. Porsev, C. Cheung, and M. S. Safronova, arXiv:2205.15484.

[26] K. Beloy, Phys. Rev. Lett. **127,** 013201 (2021).

[27] K. J. Arnold, R. Kaewuam, A. Roy, E. Paez, S. Wang, and M. D. Barrett, Phys. Rev. A **94,** 052512 (2016).

[28] T. R. Tan, R. Kaewuam, K. J. Arnold, S. R. Chanu, Z. Zhang, M. S. Safronova, and M. D. Barrett, Phys. Rev. Lett. **123,** 063201 (2019).

[29] J. Keller, D. Kalincev, T. Burgermeister, A. P. Kulosa, A. Didier, T. Nordmann, J. Kiethe, and T. E. Mehlstäubler, Phys. Rev. Appl. **11,** 011002(R) (2019).

[30] J. Keller, H. L. Partner, T. Burgermeister, and T. E. Mehlstäubler, J. Appl. Phys. **118,** 104501 (2015).

[31] P. Dubé, A. A. Madej, M. Tibbo, and J. E. Bernard, Phys. Rev. Lett. **112,** 173002 (2014).

[32] The relative difference ε of two values x_1 and x_2 is defined as $\varepsilon = ||x_1| - |x_2||/[(|x_1| + |x_2|)/2]$.

[33] C. F. Roos, Controlling the quantum state of trapped ions, Ph.D. thesis, Leopold-Franzens-Universität Innsbruck, 2000.

[34] D. Kalincev, L. S. Dreissen, A. P. Kulosa, C.-H. Yeh, H. A. Fürst, and T. E. Mehlstäubler, Quantum Sci. Technol. **6,** 034003 (2021).

[35] A. M. Hankin, E. R. Clements, Y. Huang, S. M. Brewer, J.-S. Chen, C. W. Chou, D. B. Hume, and D. R. Leibrandt, Phys. Rev. A **100,** 033419 (2019).

[36] M. Kazda, V. Gerginov, N. Huntemann, B. Lipphardt, and S. Weyers, IEEE Trans. Ultrason. Ferroelectr. Freq. Control **63,** 970 (2016).

[37] L.-S. Ma, P. Jungner, J. Ye, and J. L. Hall, Opt. Lett. **19,** 1777 (1994).

[38] D. Jiang, B. Arora, M. S. Safronova, and C. W. Clark, J. Phys. B **42,** 154020 (2009).

[39] H. S. Margolis, G. P. Barwood, G. Huang, H. A. Klein, S. N. Lea, K. Szymaniec, and P. Gill, Science **306,** 1355 (2004).

[40] A. A. Madej, P. Dubé, Z. Zhou, J. E. Bernard, and M. Gertsvolf, Phys. Rev. Lett. **109,** 203002 (2012).

[41] G. P. Barwood, G. Huang, H. A. Klein, L. A. M. Johnson, S. A. King, H. S. Margolis, K. Szymaniec, and P. Gill, Phys. Rev. A **89,** 050501(R) (2014).

[42] P. Dubé, J. Bernard, and M. Gertsvolf, Metrologia **54,** 290 (2017).

[43] B. Jian, J. Bernard, M. Gertsvolf, and P. Dubé, Metrologia **60,** 015007 (2022).

[44] CCTF, Recommendation CCTF PSFS 2 (2021): Secondary representations of the second, report of the 22nd meeting of the CCTF (session II—online) (2021).

[45] S. Hannig, L. Pelzer, N. Scharnhorst, J. Kramer, M. Stepanova, Z. T. Xu, N. Spethmann, I. D. Leroux, T. E. Mehlstäubler, and P. O. Schmidt, Rev. Sci. Instrum. **90,** 053204 (2019).

[46] K. J. Arnold, R. Kaewuam, A. Roy, T. R. Tan, and M. D. Barrett, Nat. Commun. **9,** 1650 (2018).

[47] J. Keller, T. Burgermeister, D. Kalincev, A. Didier, A. P. Kulosa, T. Nordmann, J. Kiethe, and T. E. Mehlstäubler, Phys. Rev. A **99,** 013405 (2019).